Initiation of shape-memory effect by inductive heating of magnetic nanoparticles in thermoplastic polymers

R. Mohr*, K. Kratz*, T. Weigel*, M. Lucka-Gabor†, M. Moneke†, and A. Lendlein*‡

*Institute of Polymer Research, GKSS Research Centre Geesthacht, 14513 Teltow, Germany; and †DKI, German Institute for Polymers, 64289 Darmstadt, Germany

Communicated by Robert S. Langer, Massachusetts Institute of Technology, Cambridge, MA, January 4, 2006 (received for review December 22, 2005)

In shape-memory polymers, changes in shape are mostly induced by heating, and exceeding a specific switching temperature, T_{switch}. If polymers cannot be warmed up by heat transfer using a hot liquid or gaseous medium, noncontact triggering will be required. In this article, the magnetically induced shape-memory effect of composites from magnetic nanoparticles and thermoplastic shape-memory polymers is introduced. A polyetherurethane (TFX) and a biodegradable multiblock copolymer (PDC) with poly(*p*-dioxanone) as hard segment and poly(ε-caprolactone) as soft segment were investigated as matrix component. Nanoparticles consisting of an iron(III)oxide core in a silica matrix could be processed into both polymers. A homogeneous particle distribution in TFX could be shown. Compounds have suitable elastic and thermal properties for the shape-memory functionalization. Temporary shapes of TFX compounds were obtained by elongating at increased temperature and subsequent cooling under constant stress. Cold-drawing of PDC compounds at 25°C resulted in temporary fixation of the mechanical deformation by 50–60%. The shape-memory effect of both composite systems could be induced by inductive heating in an alternating magnetic field (f = 258 kHz; H = 30 kA·m^{-1}). The maximum temperatures achievable by inductive heating in a specific magnetic field depend on sample geometry and nanoparticle content. Shape recovery rates of composites resulting from magnetic triggering are comparable to those obtained by increasing the environmental temperature.

nanocomposite | shape-memory polymer | stimuli-sensitive polymer

Shape-memory polymers are able to recover their predefined original shape when exposed to an external stimulus. A prerequisite for the shape-memory effect is a preceding functionalization of the material to temporarily fix a mechanical deformation. Most shape-memory polymers are thermosensitive materials. The shape is actuated by exceeding a specific switching temperature, T_{switch} (1). Thermoplastic shape-memory polymers have at least two separated phases, where the domains with the highest thermal transition (T_{perm}) stabilize the permanent shape by acting as physical netpoints. A second phase having another thermal transition T_{trans} serves as switch. At temperatures above T_{trans} the chain segments forming this phase are flexible and the material is highly elastic, whereas the flexibility of the chains below T_{trans} is limited and enables the fixation of the temporary shape. T_{trans} can either be a glass transition (T_g) or a melting temperature (T_m). Whereas T_{trans} is the thermal transition of the switching segment phase, typically determined by differential scanning calorimetry (DSC), T_{switch} is result of a thermomechanical test used to quantify the shape-memory effect.

An important class of thermoplastic shape-memory polymers are polyurethanes. They often contain a hard segment from methylene bis(4-phenylisocyanate) (MDI) and 1,4-butanediol. Depending on the switching segment, T_{trans} can be either a melting temperature (2) or a glass transition temperature (3, 4). Another example for shape-memory polymers with T_{trans} being a T_m are block copolymers from poly(ethylene terephthalate) and poly(ethylene oxide) (5). Compounds from shape-memory polymers and inorganic particles, including SiC particles (6, 7), carbon black (8, 9), and nanotubes (10, 11), were prepared. The incorporation of particles leads to enhanced mechanical properties (6, 8) or electric conductivity (7, 9).

Shape-memory polymers have substantial innovation potential in different application areas, e.g., as intelligent implant materials in medicine (12–14) or in smart textiles (15). If polymers cannot be warmed up by heat transfer using a hot liquid or gaseous medium, noncontact triggering will be required. Light-activation has been realized by heating thermally induced shape-memory polymers by irradiation (10, 16, 17). In addition, light-induced shape-memory polymers (18) have recently been developed, which use photosensitive functional groups as molecular switches. The magnetically induced shape-memory effect will extend the concept of noncontact triggering significantly.

In this article, we introduce magnetically induced shape-memory composites that are prepared by incorporating magnetic nanoparticles in thermoplastic shape-memory polymers. By inductive heating in an alternating magnetic field, the shape-memory effect of the composites can be triggered. Prior studies reported inductive heating of smart hydrogels (19), ferrogels (20, 21), and ferrofluids (22, 23) in alternating magnetic fields by using embedded magnetic particles (21–27). The mechanisms of heat generation are hysteresis loss and/or related processes that are direct result of superparamagnetism (23).

We show that magnetic nanoparticles can be homogeneously incorporated in the shape-memory polymer matrix. Based on the thermal and (thermo)mechanical properties of the composites, tailored programming procedures are developed. It is demonstrated that the shape-memory effect of these composite materials can be triggered magnetically. Finally, the magnetically induced recovery is quantified and compared with thermally induced recovery rates.

Results and Discussion

Formation of Composites. Two different thermoplastic shape-memory polymers were investigated as matrix material for the composites. T_{trans} of the aliphatic polyetherurethane Tecoflex EG72D (TFX) (28, 29) synthesized from methylene bis(*p*-cyclohexyl isocyanate) (H12 MDI), 1,4-butanediol (BD), and poly(tetramethylene glycol) (PTMG) (Fig. 1*a*) is a glass transi-

Conflict of interest statement: A.L. has equity in mNemoScience, which holds certain patents in the area, and serves on its scientific advisory board.

Freely available online through the PNAS open access option.

Abbreviations: DMTA, dynamic mechanical analysis at varied temperature; DSC, differential scanning calorimetry; PDC, multiblock copolymer from oligo(*p*-dioxanone)diol, oligo(ε-caprolactone)diol, and 2,2(4),4-trimethylhexanediisocyanate; TFX, polyetherurethane Tecoflex EG72D.

‡To whom correspondence should be addressed at: Institute of Polymer Research, GKSS Research Centre Geesthacht, Kantstrasse 55, 14513 Teltow, Germany. E-mail: lendlein@gkss.de.

www.pnas.org/cgi/doi/10.1073/pnas.0600079103

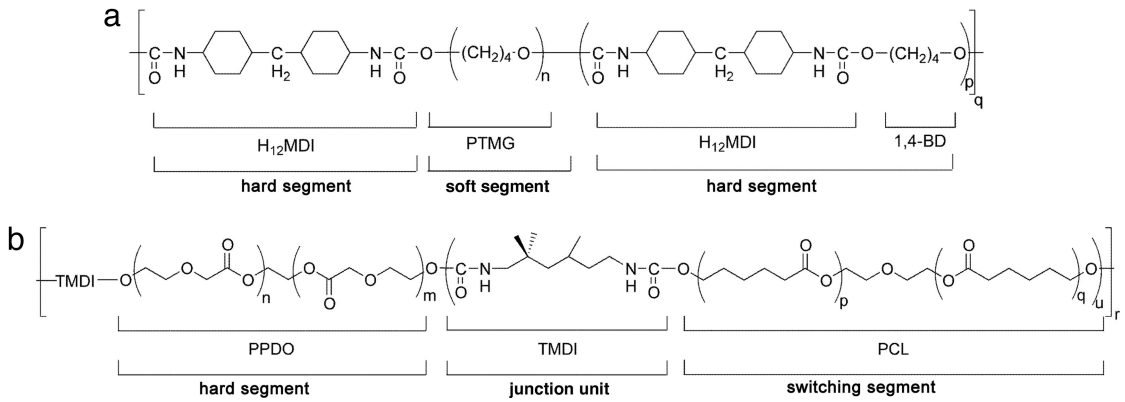

Fig. 1. Chemical structures of thermoplastic shape-memory polymers. (*a*) Polyetherurethane TFX (28), which is synthesized from methylene bis(*p*-cyclohexyl isocyanate) (H_{12} MDI), 1,4-butanediol (BD), and poly(tetramethylene glycol) (PTMG). (*b*) Multiblock copolymer PDC. PPDO, poly(*p*-dioxanone); TMDI, 2,2(4),4-trimethylhexanediisocyanate; PCL, poly(ε-caprolactone).

tion at 74°C. In addition, the multiblock copolymer PDC was selected, which is prepared from hard segment forming poly(*p*-dioxanone)diol (PPDO), switching segment forming poly(ε-caprolactone)diol (PCL) and 2,2(4),4-trimethylhexanediisocyanate (TMDI) as junction unit (12) (Fig. 1*b*). PDC has been developed for medical applications and is biodegradable. T_{trans} of PDC is a melting temperature, which is only slightly higher than body temperature to avoid any damage of surrounding tissue when heated to induce the shape-memory effect.

Iron oxide particles with average diameters at the nanoscale were chosen to support a preferably homogeneous distribution within the polymer matrix. If the composite is designed as a biodegradable biomaterial system, particle diameters in the range of 6–15 nm will have the additional advantage to be small enough for removal through extravasations or renal clearance (25).

Magnetite particles ($\varnothing$ = 20–30 nm) (30) were incorporated in TFX by an extrusion process. X-ray computer-tomographic investigations of the resulting composites indicated the formation of particle agglomerates in the range of micrometers (Fig. 6, which is published as supporting information on the PNAS web site). A homogeneous distribution of nanoparticles within the TFX polymer matrix could be achieved with particles having an iron(III)oxide core embedded in a matrix of silica (31) (Fig. 2). The silica apparently improves the compatibility between the two composite components. The black points in Fig. 2*b* are the iron oxide domains embedded into silica matrix (dark gray wrapping). The few agglomerates, which are occasionally observed in the composite structure, could be formed by compression of the mixed component, which has not yet melted in the feed zone of the extruder. To minimize influences from irregularities in the particle distribution within the polymer matrix, investigations on thermal and mechanical properties as well as on the shape-memory functionalization are focused on composites with the iron(III)oxide/silica particles.

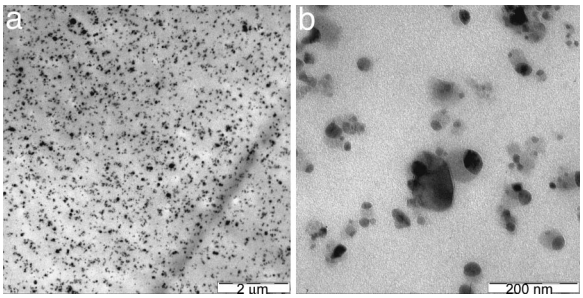

Fig. 2. Transmission electron microscopy pictures of TFX100 with 10 wt % particle content. (Scale bars: *a*, 2 μm; *b*, 200 nm.)

Thermal and (Thermo)Mechanical Properties of Nanocomposites. The influence of the particle content on the thermal and (thermo)-mechanical properties was investigated by DSC, tensile tests, and dynamic mechanical analysis at varied temperature (DMTA).

In the DMTA measurements of all TFX materials, a broad peak was observed in the tan δ-curve with a maximum at 74°C, which is attributed to the glass transition of the switching phase. In the temperature range of 120–140°C a second thermal transition was found, which is related to the hard segment (Fig. 7*b*, which is published as supporting information on the PNAS web site). Both thermal transitions are not affected by the incorporation of particles.

The tensile tests were performed for TFX samples at 25°C and at T_{high} = 80°C (Table 1). At 25°C the mechanical properties of TFX and the different TFX composites are similar. Only a slight decrease in elastic modulus was observed for the highest particle content.

At T_{high} = 80°C, TFX materials are significantly softer. Elongation at break ε_b increases with growing particle content. The material properties at T_{high} are predominantly determined by the hard segment. Therefore, it is speculated that particles reduce the interaction between polyurethane segments.

PDC consist of two crystallizable segments: poly(*p*-dioxanone) and poly(ε-caprolactone). In the thermograms obtained from DSC, four thermal transitions are observed (Table 4, which is published as supporting information on the PNAS web site). The glass transition $T_{g,1}$ at −60°C is attributed to amorphous PCL-chains, and $T_{g,2}$ at −12°C is related to amorphous poly(*p*-dioxanone)diol. $T_{m,1}$ at 39°C corresponds to crystallites of the PCL phase, and $T_{m,2}$ at 93°C is attributed to the hard segment phase. Peak maxima of tan δ at −62°C and −12°C observed in DMTA are in good agreement with DSC results (Fig. 7*a*). Glass transition temperatures as well as melting points are not affected by incorporation of nanoparticles.

Tensile tests were performed at 25°C and at T_{high} = 55°C (Table 2). The mechanical properties at 25°C are identical for PDC and the PDC composites. The values for the elastic modulus is in the range of 130–150 MPa, and the elongation at break ε_b decreased from 660% for PDC to 460% with increasing particle content (Table 2). At T_{high} = 55°C PCL segments are amorphous and E module is lowered by ≈70–75% compared with room temperature.

The influence of particle content on ε_b at T_{high} is different for

Table 1. Mechanical and thermal properties of TFX and TFX composites determined by tensile test and DMTA

	25°C				80°C				
Sample ID*	E, MPa	σ_m, MPa	ε_b, %	E', MPa	E, MPa	σ_m, MPa	ε_b, %	E', MPa	T_{trans} $T_{max,\delta}$, °C
TFX000	396	57	320	1,220	7	4	650	11	74
TFX050	270	52	380	1,180	3	1.5	1,200	11	74
TFX075	295	52	320	1,110	3	nd	nd	11	74
TFX100	138	57	420	1,110	4	nd	nd	10	74

E is the elastic modulus (Young's modulus), σ_m is the maximum stress, ε_b is the elongation at break, E' is the storage modulus, $T_{max,\delta}$ is the temperature at peak maximum of tan δ determined by DMTA, and T_{trans} is the thermal transition of the switching segment phase. nd, not determined, geometrical limit of the tensile tester for maximum deformation is reached before the sample breaks.
*The three-digit number gives the particle content in wt % × 10.

PDC and TFX materials. This observation needs to be taken into account for selecting suitable programming procedures.

Inductive Heating in Alternating Magnetic Field. Inductive heating of the composites was investigated to determine the temperatures, which can be reached within a magnetic field characterized by its field strength H being a function of location (Fig. 8, which is published as supporting information on the PNAS web site). As soon as the magnetic field is switched on, the sample's temperature begins to increase. Within a few minutes the temperature measured at the sample surface reaches a constant level that is characterized by the maximum achievable temperature T_{max}. T_{max} depends on the sample geometry characterized by surface to volume ratio, S/V (Fig. 3), and results from an equilibrium between heat generation and heat transfer to the environment. The smaller the S/V ratio, the higher is the achievable temperature and the slope of the heating curve. T_{max} increases with the particle content and the magnetic field strength. Temperatures up to 88°C were obtained for TFX100 (Fig. 4).

Shape-Memory Properties. The magnetically induced shape-memory effect is exemplarily demonstrated for composite TFX100 in Fig. 5 and Movie 1 (which is published as supporting information on the PNAS web site), where a change in shape from a corkscrew like spiral (temporary shape) to a plane stripe (permanent shape) occurring within 22 s is shown. Shape-memory properties of the TFX samples were investigated by cyclic thermomechanical tests (12). Results of cyclic thermomechanical experiments for pure TFX-polymer and TFX100 are shown in Fig. 9, which is published as supporting information on the PNAS web site. At first, the sample is elongated at temperature T_{high}, which is higher than T_{switch} but lower than the thermal transition of the hard segment, T_{perm}. To allow relaxation, strain is kept constant for a certain time interval. The elongated sample is now cooled for fixation of the temporary shape. This step is performed under stress control, which results in an increase of strain as a consequence of entropy elasticity. Once the switch phase is glassy, strain decreases with temperature because of thermal contraction. Finally, the shape-memory effect is initiated by reheating under stress control conditions.

The effect can be quantified by using two characteristic factors. The shape fixity rate $R_f(N)$ describes the ability of the switching segment to fix the mechanical deformation, which is applied during the programming process. $R_f(N)$ is defined as the quotient of the elongation in the tension-free state after cooling to T_{low} $\varepsilon_u(N)$ of cycle N and the extension ε_m, which is a programming parameter.

$$R_f(N) = \varepsilon_u(N)/\varepsilon_m. \quad [1]$$

For TFX composites, R_f (1) values between 100% and 118% are determined (Table 3).

The recovery of the original shape is quantified by the shape recovery rate, which was calculated from $\varepsilon_u(N)$ and the extension at the tension-free states $\varepsilon_P(N-1)$ and $\varepsilon_P(N)$ while expanding the sample in two subsequent cycles $N-1$ and N.

$$R_r(N) = \frac{\varepsilon_u(N) - \varepsilon_p(N)}{\varepsilon_u(N) - \varepsilon_p(N-1)}. \quad [2]$$

The TFX materials have shape recovery ratios of ≈80% in the first cycle, independent from the particle content.

Limitations in the elasticity of PDC composites at T_{high} require an alternative programming procedure. Programming by cold-drawing (32) enabled the realization of comparable deformations ε_u to those applied for TFX (Table 3). The sample was elongated at T_{deform} = 25°C, which is below the thermal transition of the switching segment T_{trans}. Fixation of the temporary shape is caused by strain-induced crystallization and strain-oriented reorganization. Shape fixity rates between 50% and 60% were reached for PDC materials. Thus the shape fixity rates achieved by applying cold-drawing for pure PDC polymer is ≈40–50% lower compared with the programming by deformation at T_{high} (12), which is caused by the loss of the rubber elastic part of the deformation after external stress was released. The recovery experiments were performed at T_{high} = 55°C. Shape recovery rates are between 47% and 65% for samples programmed by cold-drawing.

For magnetically induced recovery experiments, TFX composite samples were programmed by deformation at T_{high} = 80°C, as described above, and PDC composite samples by

Table 2. Mechanical and thermal properties of PDC and PDC composites determined by tensile test and DMTA

	25°C				55°C				
Sample ID*	E, MPa	σ_m, MPa	ε_b, %	E', MPa	E, MPa	σ_m, MPa	ε_b, %	E', MPa	T_{trans} $T_{m,1}$, °C
PDC000	145	22	660	170	29	9	600	60	39
PDC050	132	15	460	220	30	4	40	72	39
PDC100	150	15	470	170	37	4	40	76	39

E is the elastic modulus (Young's modulus), σ_m is the maximum stress, ε_b is the elongation at break, E' is the storage modulus determined by DMTA, T_m is the melting temperature determined by DSC, and T_{trans} is the thermal transition of the switching segment phase.
*The three-digit number gives the particle content in wt % × 10.

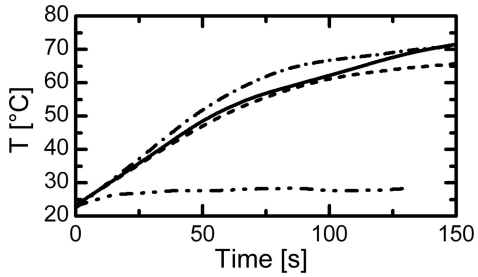

Fig. 3. Heating curves for samples with different S/V ratios. $f = 258$ kHz, $H = 12.6$ kA·m^{-1}. –·–·–·–, $S/V = 1.4$; ——, $S/V = 1.5$; - - - -, $S/V = 1.6$; –··–··–, $S/V = 8.1$.

cold-drawing. S/V-ratio of the specimen was adjusted to reach a temperature above T_{switch} but below T_{perm}.

The results of the magnetically induced shape recovery rates $R_{r,mg}$ (Table 4) give evidence that magnetically and thermally induced shape recovery results are comparable. As a control experiment, pure polymer samples were exposed to the alternating magnetic field. As expected, the temperature of these samples did not change.

Speculation About Potential Applications. Magnetically triggered shape-memory composites have an high application potential in medicine. Smart implants or instruments could enable surgeons to perform mechanical adjustments in a noncontact mode. Examples given in the patent literature include smart catheters (33) or intelligent implants for treating ocular hypertension (34). Another area of applications could be on-demand drug delivery from an implanted depot, which could be triggered noninvasively by a magnetic field. Especially, the PDC composite system is suitable to be further developed into a medical application, because the PDC polymer has been developed as a degradable biomaterial, and T_{trans} of the PDC materials is slightly above body temperature.

Conclusions

Noncontact triggering of shape changes in polymers has been realized by incorporating magnetic nanoparticles in shape-memory polymers and inductive heating of these compounds in alternating magnetic fields. Magnetic nanoparticles having an iron(III)oxide core in silica matrix could be incorporated in the thermoplastic shape-memory polymers PDC and TFX. Whereas introduction of nanoparticles in TFX having an amorphous switching phase improved the elastic properties even at increased temperature, the contrary effect was observed for PDC having a crystallizable switching segment. Despite the relatively low ε_b at elevated temperature, elongations between 57% and 85% could be temporarily fixed for PDC by cold-drawing at

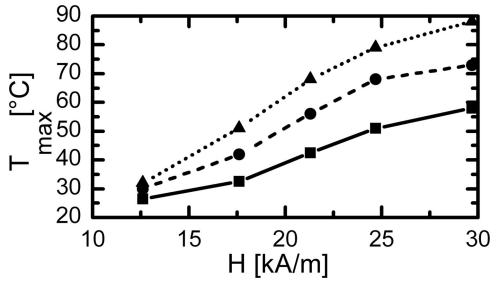

Fig. 4. Temperatures achieved for TFX composites when exposed to magnetic field depending on particle content and magnetic field strength. $f = 258$ kHz, sample size length = 30.0 mm; thickness = 0.3 mm; width = 4.0 mm; T_{max} is the maximum temperature achieved by inductive heating. —■—, 5 wt % particle content; --●--, 7.5 wt % particle content; ··▲··, 10 wt % particle content.

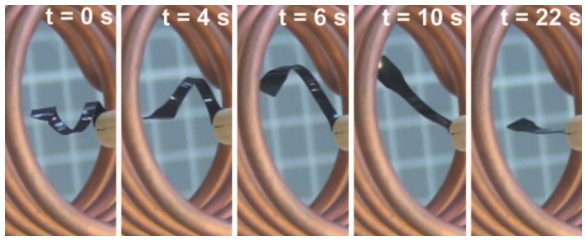

Fig. 5. Series of photographs showing the macroscopic shape-memory effect of TFX100 composite with 10 wt % particle content. The permanent shape is a plane stripe of composite material, and the temporary shape is a corkscrew-like spiral. The pictures show the transition from temporary to permanent shape in a magnetic field of $f = 258$ kHz and $H = 30$ kA·m^{-1} in an inductor. Movie 1 shows the shape change.

25°C. For both compound systems, shape recovery rates obtained by magnetically induced actuation are comparable with those reached by increasing the environmental temperature.

Potential applications for magnetically induced shape-memory composites include smart implants and controlled medical instruments.

Materials and Methods

Thermoplastic Shape-Memory Polymers. Cycloaliphatic TFX was purchased from Noveon (Wilmington, MA).

Multiblock copolymer (PDC) has been synthesized from oligo(*p*-dioxanone)diol, oligo(ε-caprolactone)diol, and 2,2(4),4-trimethylhexanediisocyanate, as a junction unit according to ref. 12. The weight average molecular weight, M_w, was 110,000. The hard segment content was 67 wt %.

Nanoparticles. Nanoscaled particles AdNano MagSilica 50 were provided by Degussa Advanced Nanomaterials (Degussa, Hanau, Germany). The particles consist of an iron(III)oxide (Fe_2O_3; CAS no. 1309-37-1) core in a silica matrix (SiO_2; CAS no. 7631-86-9). The mean aggregate size (photon correlation spectroscopy of an aqueous dispersion) was 90 nm, the mean domain size (x-ray diffraction) was 20–26 nm, and the domain content (x-ray fluorescence analysis) was 50–60 wt %. The particles had a surface area of 50–65 m^2·g^{-1} and a saturation magnetization of 22–32 A·m^2·kg^{-1}. The density was in the range of 2.5–3.5 g·cm^{-3}.

Nanoscaled particles iron(II,III)oxide (Fe_3O_4; CAS no. 1317-61-9) were purchased from Sigma-Aldrich. The spherical particles had a particle size of 20–30 nm, a surface area of >60 m^2·g^{-1}, and a density of 4.8–5.1 g·cm^{-3}.

Preparation of Polymer Composites. ***TFX composites.*** Compounding of nanocomposites was carried out with a co-rotating twin screw extruder HAAKE PolyLab system (PTW 16/25; Thermo Electron Corporation). The processing temperature was in the range between 165°C and 170°C. Before the processing, the materials were milled, mixed, and dried in a vacuum oven at 65°C for 4 h. Extrusion was performed at screw speeds of 100 and 150 rpm. ***PDC composites.*** PDC-based compounds were performed in a small conical counter rotating twin screw extruder HAAKE PolyLab system (Rheomex CTW5; Thermo Electron Corporation). PDC was gravimetrically mixed with the nanoparticles before extrusion. After starting the extruder, the material was filled in the hopper. When the pressure rises in the back-flow channel, the mixing time started. The processing temperature was 160°C, and the screw speed was 150 rpm.

Morphology Characterization. Transmission electron microscopy analysis was conducted by using a Zeiss 909/50 at different magnification levels. Images were captured from ultrathin spec-

Table 3. Strain fixity and strain recovery rates for cycle $N = 1$

		Thermally induced recovery			Magnetically induced recovery		
Sample ID*	ε_m, %	$\varepsilon_u(1)$, %	$R_f(1)$, %	$R_r(1)$, %	$\varepsilon_u(1)$, %	$R_f(1)$, %	$R_{r,mg}(1)$, %
TFX000	50	50†	100†	80†	50‡	100	0
TFX050	50	49†	98†	81†	59‡	118	38§
TFX075	50	49†	98†	82†	54‡	108	88
TFX100	50	50†	100†	78†	53‡	106	91
PDC000¶	100	50	50	50‖	50	50	0
PDC000¶	150	75	50	47‖	75	50	0
PDC100¶	100	57	57	59‖	57	57	65
PDC100¶	150	85	57	65‖	91	60	68

ε_u is the elongation achieved at stress zero after cooling to T_{low}, R_f is the strain fixity rate, R_r is the strain recovery rate calculated according to Eqs. **1** and **2**, and $R_{r,mg}$ is the strain recovery rate obtained by inductive heating in the magnetic field.

*The three-digit number gives the particle content in wt % × 10.

†Cyclic thermomechanical experiments $T_{high} = 80°C$; $T_{low} = 0°C$.

‡Programming including deformation at $T_{high} = 80°C$.

§T_{switch} not completely reached.

¶Programming by cold-drawing.

‖Shape recovered at 55°C.

imens of 50 nm of the material samples, which were prepared with a Leica Ultracut UCT microtome. Microtomographic investigations were conducted by using a SkyScan (Aartselaar, Belgium) 1072 x-ray microtomograph.

DSC. DSC experiments were performed on a Netzsch (Selb, Germany) DSC 204. All experiments were performed with a constant heating and cooling rate of 10 K·min^{-1}. Whenever a maximum or minimum temperature in the testing program was reached, this temperature was kept constant for 2 min. The PDC samples were investigated in the temperature range from −80°C to 150°C. The sample was heated from 20°C to 150°C, then cooled down to −80°C and again warmed up to 150°C. The melting temperature was determined from the first heating cycle, and the glass transition temperature was determined from the second heating run. The TFX samples were investigated in the temperature range from −50°C to 200°C.

DMTA. The determination of the dynamic mechanical properties was performed on a Gabo (Ahlden, Germany) Eplexor 25 N. All experiments were performed in temperature sweep mode with a constant heating rate of 2 K·min^{-1}. The oscillation frequency was 10 Hz. PDC samples were investigated in the temperature interval from −100°C to 100°C. TFX samples were investigated from 0°C to 200°C. $T_{max,\delta}$ is the maximum peak temperature of the tan δ curve.

Tensile Tests and Cyclic Thermomechanical Experiments. Tensile tests at room temperature were carried out on Zwick (Ulm, Germany) Z005 and Z2.5 tensile testers. Experiments at extended temperature and thermomechanical tests were performed on Zwick Z1.0 and Z005 tensile testers equipped with thermo chambers and temperature controller (Eurotherm Regler, Limburg, Germany). The strain rate was 5 mm·min^{-1} in all experiments.

Test specimens for mechanical characterization were processed on a polymer press (type 200 E; Dr. Collin, Ebersberg, Germany). TFX materials were processed at 170°C under a pressure of 100 bar for 5 min. Processing parameters for the PDC materials were 100°C and 100 bar for 5 min. The film thickness typically was 0.3 mm for the cyclic, thermomechanical experiments and 0.5–0.6 mm for measurements in the magnetic field. Specimen type no. 1BB according to European Standard for tensile test (35) was cut with a punching tool, $l_o = 20$ mm and width = 2 mm.

Programming of PDC materials by cold-drawing. PDC samples were programmed by cold-drawing at $T_{deform} = 25°C$ by stretching to ε_m. After keeping this deformation for 5 min to allow relaxation, stress was released to 0 MPa.

Programming of TFX materials by deformation at T_{high}. The sample is deformed to $\varepsilon_m = 50\%$ at $T_{high} = 80°C$. After keeping this deformation for 5 min to allow relaxation, the stress was held constant while the sample was cooled to $T_{low} = 0°C$, whereby the temporary shape is fixed. Stress was then completely removed.

Thermally induced recovery procedure. The thermally induced shape recovery experiment was performed by heating the sample to T_{high} (PDC, 55°C; TFX, 80°C) in an oven for 10 min.

Magnetically induced recovery procedure. For magnetically induced recovery the programmed samples were exposed to a magnetic field with a field strength of 30 kA·m^{-1} in the center of the coil, and a frequency of 258 kHz.

Cyclic thermomechanical tensile test. In a first step, the sample was deformed to $\varepsilon_m = 50\%$ at $T_{high} = 80°C$. After keeping this deformation for 5 min to allow relaxation, the stress was held constant while the sample was cooled to $T_{low} = 0°C$, whereby the temporary shape was fixed. Then stress was lowered to zero. The sample now was in its temporary shape. Finally, the sample was warmed up again to $T_{high} = 80°C$ with a heating rate of 2 K·min^{-1}. After waiting for 10 min, the next cycle was performed.

Magnetic Field Application. Inductive heating was accomplished by positioning the sample in an alternating magnetic field at a frequency of $f = 258$ kHz. The equipment consisted of a high-frequency generator (TIG 5/300; Huettinger Electronic, Freiburg, Germany), a water-cooled coil with a diameter of 4 cm with 6 loops, and an IR pyrometer (Metis MY84, Sensortherm; Frankfurt) for noncontact measuring of the sample temperature. This experimental setup allows one to infinitely vary the magnetic field strengths in the center of the coil between 7 and 30 kA·m^{-1} by adjusting the power output of the generator. Details about the determination of the magnetic field strength are available in Fig. 8.

We thank H. Kosmella (Institute of Polymer Research) for assistance with (thermo)mechanical tests, M. Zierke for assistance with synthesis, and F. Klein for assistance with processing PDC. We thank Degussa Advanced Nanomaterials for providing material samples of AdNano MagSilica 50. This work was supported by Arbeitsgemeinschaft industrieller Forschungseinrichtungen AZ VI A2-404245/2 initiative program Zukunftstechnologien für kleine und mittlere Unternehmen.

1. Lendlein, A. & Kelch, S. (2002) *Angew. Chem. Int. Ed.* **41,** 2034–2057.
2. Kim, K., Lee, S. Y. & Xu, M. (1996) *Polymer* **37,** 5781–5793.
3. Takahashi, T., Hayashi, N. & Hayashi, S. (1996) *J. Appl. Polym. Sci.* **60,** 1061–1069.
4. Lin, R. & Chen, L. W. (1998) *J. Appl. Polym. Sci.* **69,** 1563–1574.
5. Luo, X., Zhang, X., Wang, M., Ma, D., Xu, M. & Li, F. (1997) *J. Appl. Polym. Sci.* **64,** 2433–2440.
6. Liu, Y., Gall, K., Dunn, M. L. & McCluskey, P. (2004) *Mech. Mater.* **36,** 929–940.
7. Gall, K., Dunn, M. L., Liu, Y., Finch, D., Lake, M. & Munshi, N. A. (2002) *Acta Mater.* **50,** 5115–5126.
8. Li, F., Qi, L., Yang, J., Xu, M., Luo, X. & Ma, D. (2000) *J. Appl. Polym. Sci.* **75,** 68–77.
9. Yang, B., Huang, W. M., Li, C. & Chor, J. H. (2005) *Eur. Polym. J.* **50,** 1123–1128.
10. Cho, J. W., Kim, J. W., Jung, Y. C. & Goo, N. S. (2005) *Macromol. Rapid Commun.* **26,** 412–416.
11. Koerner, H., Price, G., Pearce, N. A., Alexander, M. & Vaia, R. A. (2004) *Nat. Mater.* **3,** 115–120.
12. Lendlein, A. & Langer, R. (2002) *Science* **296,** 1673–1676.
13. Lendlein, A. & Kelch, S. (2005) *Clin. Hemorheol. Microcirc.* **32,** 105–116.
14. Metcalfe, A., Desfaits, A.-C., Salazkin, I., Yahia, L., Sokolowski, W. M. & Raymond, J. (2003) *Biomaterials* **24,** 491–497.
15. Hu, J., Ding, X., Tao, X. & Yu, J. (2002) *J. Dong Hua Univ. (Engl. Ed.)* **19,** 3.
16. Maitland, D. J., Metzger, M. F., Schumann, D., Lee, A. & Wilson, T. S. (2002) *Lasers Surg. Med.* **30,** 1.
17. Maitland, D. J., Wilson, T., Metzger, M. & Schumann, D. L. (2002) *Proc. SPIE Int. Soc. Opt. Eng.* **4626,** 394–402.
18. Lendlein, A., Jiang, H., Jünger, O. & Langer, R. (2005) *Nature* **434,** 879–882.
19. Mitwalli, A. H., Denison, T., Jackson, D. K., Leeb, S. B. & Tanaka, T. (1997) *J. Int. Mater. Syst. Struct.* **8,** 596–604.
20. Zrínyi, M., Barsi, L. & Büki, A. (1996) *J. Chem. Phys.* **104,** 8750.
21. Lao, L. L. & Ramanujan, R. V. (2004) *J. Mater. Sci. Mater. Med.* **15,** 1061–1064.
22. Ma, M., Wu, Y., Zhou, J., Sun, Y., Zhang, Y. & Gu, N. (2004) *J. Magn. Magn. Mater.* **268,** 33–39.
23. Hergt, R., Andrä, W., d'Ambly, C. G., Hilger, I., Kaiser, W. A., Richter, U. & Schmidt, H.-G. (1998) *IEEE Trans. Magn.* **34,** 3745–3754.
24. Hilger, I., Hergt, R. & Kaiser, W. A. (2005) *IEEE Proc. Nanobiotechnol.* **152,** 33–39.
25. Gupta, A. K. & Gupta, M. (2005) *Biomaterials* **26,** 3995–4021.
26. Müller, R., Hergt, R., Zeisberger, M. & Gawalek, W. (2005) *J. Magn. Magn. Mater.* **289,** 13–16.
27. Jordan, A., Rheinländer, Th., Waldöfner, N. & Scholz, R. (2003) *J. Nanopart. Res.* **5,** 597–600.
28. Guignot, C., Betz, N., Legendre, B., Le Moel, A. & Yagoubi, N. (2001) *Nucl. Instrum. Meth. Phys. Res. B* **185,** 100–107.
29. Lamba, N. M., Woodhouse, K. & Cooper, S. (1998) *Polyurethanes in Biomedical Applications* (CRC, Boca Raton, FL).
30. Schwertmann, U. & Cornell, R. M. (1991) *Iron Oxides in the Laboratory: Preparation and Characterization* (VCH, Weinheim, Germany)
31. Gottfried, H., Janzen, C., Pridoehl, M., Roth, P., Trageser, B. & Zimmermann, G. (2003) U.S. Patent 6,746,767.
32. Ping, P., Wang, W., Chen, X. & Jing, X. (2005) *Biomacromolecules* **6,** 587–592.
33. Wilson, T., Maitland, D., Schumann, D. L., Little, S. L. & Ahre, P. E. (2003) U.S. Patent Appl. 2,003,236,533.
34. Shadduck, J. H. (2004) U.S. Patent Appl. 2,004,193,262.
35. European Standard EN ISO 527-2 (1996).